

# Effect of heat treatment on the structure and fatigue behaviour of austenitic Fe–Ni alloy

K.J. Ducki\*, M. Cieśla

Department of Materials Science, Silesian University of Technology,  
ul. Krasińskiego 8, 40-019 Katowice, Poland

\* Corresponding author: E-mail address: kazimierz.ducki@polsl.pl

Received 19.03.2008; published in revised form 01.09.2008

## Properties

### ABSTRACT

**Purpose:** The paper addresses the problem of determining the dependence between initial heat treatment of an austenitic Fe–Ni alloy and its fatigue life at room and elevated temperature. Specimens of Fe–Ni alloy were subject to tests after two variants of heat treatment: solution heat treatment followed by typical single-stage ageing, and solution heat treatment followed by novel two-stage ageing.

**Design/methodology/approach:** For the investigated Fe–Ni alloy after solution heat treatment in the conditions: 980°C/2h/water, two variants of specimen ageing were applied for comparison, i.e. single-stage ageing (715°C/16h/air) and two-stage ageing (720°C/8h + cooling in the furnace up the temperature of 650°C + 650°C/8h/air). Specimens that underwent heat treatment were subjected to a static tensile test and low-cycle fatigue tests (LCF), carried out at room temperature and at an increased temperature of 600°C.

**Findings:** It has been found that, at both tested temperatures, the specimens of Fe–Ni alloy after two-stage ageing are distinguished by higher strength properties with a little lower plastic properties. In a case of low-cycle fatigue tests carried out at a temperature of 20°C and 600°C, specimens after single-stage ageing were characterized by higher fatigue life. Lower fatigue life of Fe–Ni alloy after two-stage ageing can be explained by increased brittleness of material in boundary areas.

**Practical implications:** The fatigue life results obtained in LCF conditions can be used in predicting the duration of operation of products made out of Fe–Ni alloy both in room and elevated temperatures.

**Originality/value:** The significance of the applied ageing variants' effect on the mechanical properties and fatigue life of the tested austenitic Fe–Ni alloy is shown in the paper.

**Keywords:** Fatigue; Metallic alloys; Heat treatment; Structure

## 1. Introduction

Austenitic Fe–Ni alloys precipitation-strengthened with intermetallic phases of type  $\gamma'$  [Ni<sub>3</sub>(Al,Ti)] are characterised by various characteristic properties, such as [1-5]: high mechanical properties, considerable creep resistance and heat resistance at slightly elevated and high temperatures, excellent corrosion resistance, high ductility at low temperatures, and are non-magnetic. The temperature range, within which these alloys can be used,

spreads from the temperature of liquid helium (–269°C) up to temperature within a range of 540–815°C. This modern group of metallic materials is more and more widely utilised in the conventional power industry and nuclear power engineering, aeronautical engineering, chemical and petrochemical industry, cryogenic engineering and for tools in nonferrous metals processing.

High-temperature Fe–Ni alloys obtain their optimum properties after multi-stage heat treatment consisting of solution heat treatment (or annealing) and various ageing variants. Most frequently for such type of alloys, solution heat treatment from

a temperature of circa 1000°C in water or oil and ageing at temperature of 710-730°C during 16-20 h with subsequent cooling in the air are applied [6, 7]. For some Fe–Ni alloys (for instance Inconel 706 and 901) after solution heat treatment, it is recommended to apply two-stage ageing, which consists of carrying out a controlled cooling cycle between two isothermal soaking processes [8]. Such processing is aimed at obtaining optimum values and distribution of precipitates of the  $\gamma'$  type intermetallic phase, which ensures maximum strength coupled with good alloy plasticity under creep conditions at a temperature of 650-700°C.

In the presented paper, investigation was initiated concerning the effect of initial heat treatment on the structure, mechanical properties and fatigue life at room and elevated temperature of an austenitic Fe–Ni alloy precipitation-strengthened with an intermetallic phase of the  $\gamma'$  type. Specimens of Fe–Ni alloy were subject to tests after two variants of heat treatment, i.e. solution heat treatment followed by typical single-stage ageing, and solution heat treatment followed by novel two-stage ageing. The paper constitutes continuation of the research [9-12] on the structure and properties of austenitic Fe–Ni alloys precipitation-strengthened with intermetallic phases.

## 2. Material and procedure

The examinations were performed on rolled bars, 16 mm in diameter, of an austenitic Fe–Ni alloy. The chemical composition of the material is given in Table 1.

Specimens of Fe–Ni alloy were subjected to tests after two variants of heat treatment, i.e. solution heat treatment and single-stage ageing (variant A) and solution heat treatment followed by two-stage ageing (variant B). Parameters of heat treatment for the investigated Fe–Ni alloy were determined based on the previously carried out studies [9-12] and data from professional literature [6-8]. For the investigated alloy after solution heat treatment in the conditions: 980°C/2h/water, two variants of specimens' ageing were used for comparison, i.e.:

- single-stage ageing (variant A): 715°C/16h/air;
- two-stage ageing (variant B): 720°C/8h + cooling in the furnace up to a temperature of 650°C + 650°C/8h/air.

A schematic course of heat treatment of specimens made of the investigated alloy is presented in Fig. 1.

A static tensile test at room temperature was carried out using a strength testing machine MTS-810. Cylindrical five-time specimens with a diameter  $d_0 = 10$  mm and measuring length  $l_0 = 50$  mm were used for the tests. A yield strength (Y.S), tensile strength (T.S), unit elongation (EL.) and reduction of area (R.A) were determined.

Low-cycle fatigue tests were carried out at room temperature and a temperature of 600°C using a servo-hydraulic system, MTS-810. The tests were carried with the servo-hydraulic machine being controlled by strain (the so-called fixed control) for the range of total strain  $\Delta\epsilon_i$  from 0.6 to 1.4 %. In a sinusoidal deformation cycle, an average strain rate  $\dot{\epsilon} = 1.5 \times 10^{-5} \text{ s}^{-1}$  was

applied. The number of cycles until failure of specimen  $N_f$  was assumed to be the criterion of the investigated materials' durability [13-16]. Cylindrical specimens with a diameter  $d_0 = 12$  mm and measuring length  $l_0 = 30$  mm were used for tests.

Heating of the specimens examined at 600°C was performed with the use of Lepel induction heater (power 12.5 kVA, frequency 450 kHz) and a cylindrical inductor with a shape selected so as to obtain a possibly uniform temperature distribution along the specimen length limited by a sensor base. During the test, the specimens' temperature was controlled by thermocouples (PtRh–Pt) welded to the specimen surface to an accuracy of  $\pm 5^\circ\text{C}$ .

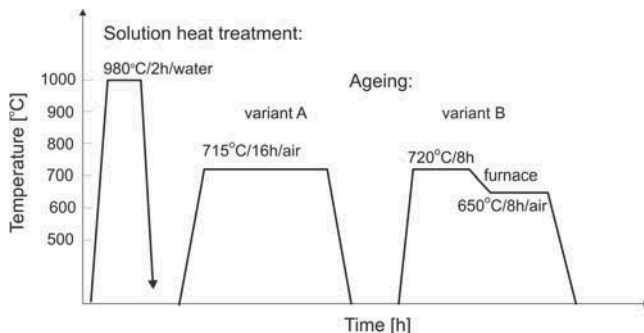


Fig. 1. Diagram of heat treatment of specimens of A and B variants of the investigated Fe–Ni alloy

Specimens' structural tests were conducted on a Reichert MeF-2 light microscope. The surface of specimens with diameters of 10 and 12 mm was initially ground on a disc grinder and next, on waterproof abrasive papers with graining of 80-2000. Final surface processing consisted of polishing with diamond paste on a semi-automatic Struers grinding machine. The specimens were etched using a reagent with the following composition: 54 cm<sup>3</sup> of hydrofluoric acid (HF), 8 cm<sup>3</sup> of nitric acid (HNO<sub>3</sub>) and 38 cm<sup>3</sup> of distilled water.

Tests of the specimens' substructure were carried out using a thin foil technique on a Jeol transmission electron microscope, JEM-2000 FX, at accelerating voltage of 160 kV. The discs for thin foils with a diameter of 3.0 mm and thickness of about 0.5 mm were cut out from a previously prepared shaft, 3.0 mm in diameter, by means of a Struers' cutting-off machine, Acutom. The discs were initially ground with waterproof abrasive papers until the thickness of ca. 0.05 mm was obtained. The so obtained discs were then thinned via two-sided jet electrolytic polishing method in a Tenupol-3 device of Struers manufacture. A company brand reader A-8 was used (for alloys with a Fe matrix) cooled down to a temperature 15°C at polishing voltage of 80 V.

A Jeol JSM-35 scanning microscope was used for the observation of specimens' fractures. The aim of the observation was a fatigue analysis of the fractured specimens produced during the low-cycle fatigue tests. The surfaces of the specimens' scrap after a static tensioning test at room temperature were observed as well.

Table 1.

Chemical composition of the investigated Fe–Ni austenitic alloy

Content of an element, wt. %															
C	Si	Mn	P	S	Cr	Ni	Mo	V	W	Ti	Al	Co	B	N	Fe
0.05	0.55	1.25	0.026	0.016	14.3	24.5	1.34	0.41	0.10	1.88	0.16	0.08	0.007	0.0062	55.32

### 3. Experimental results

The results of specimens' microscope observations of the Fe–Ni alloy after both variants of thermal treatment are presented in Figs. 2 and 3. In both cases, the initial alloy structure demonstrated an austenitic matrix with a diversified grain size and with numerous twin systems as well as particles of primary and secondary precipitates.

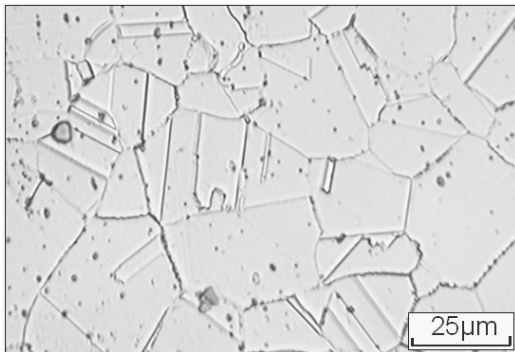


Fig. 2. Alloy structure after solution heat treatment and ageing according to variant A. Austenite with a diversified grain size, with primary and secondary precipitates

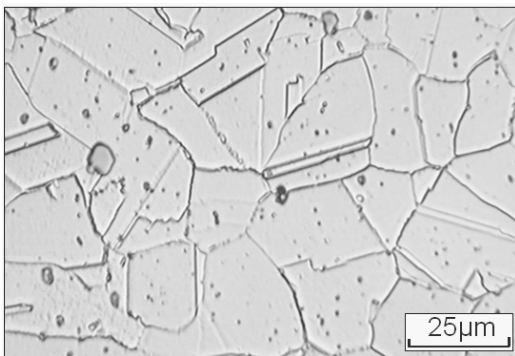


Fig. 3. Alloy structure after solution heat treatment and ageing according to variant B. Austenite with a diversified grain size, with primary and secondary precipitates

By comparing both of the Fe–Ni alloy structures, it can be assumed that in the alloy after 2-stage ageing (variant B), a higher fraction of secondary phase particle precipitates is observed on grain boundaries in relation to 1-stage ageing (variant A).

This finding is corroborated by the results of research on the Fe–Ni alloy substructure conducted using a transmission electron microscope (Figs. 4 and 5). It has been found that the precipitation process in the alloy substructure for variant A took place mainly within the matrix, where a characteristic “tweed-like” contrast connected with the occurrence of coherent particles of the intermetallic phase type  $\gamma'$  [ $\text{Ni}_3(\text{Al},\text{Ti})$ ] was identified (Fig. 4). As for variant B, the precipitation process of secondary phase particles took place both within the matrix and along the grain boundaries (Fig. 5). Early stages of type  $\gamma'$  phase precipitates were observed in

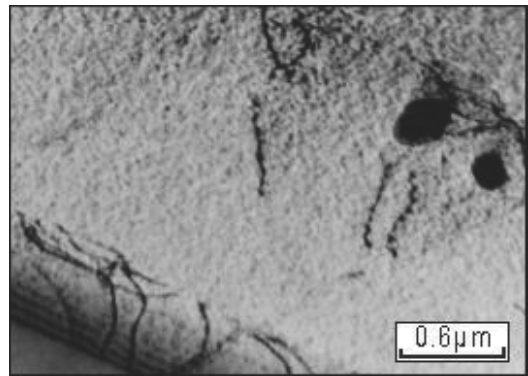


Fig. 4. Alloy substructure after heat treatment according to variant A. Coherent precipitates of phase  $\gamma'$  and lenticular particles of phase G in the matrix

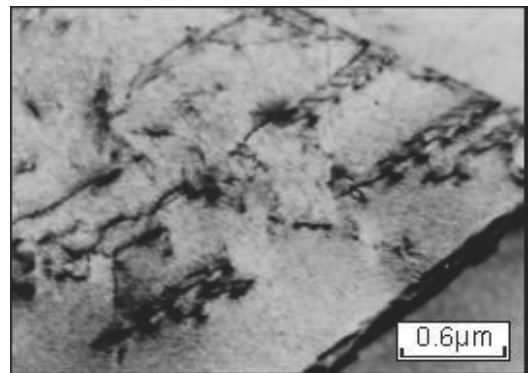


Fig. 5. Alloy substructure after heat treatment according to variant B. Coherent precipitates of phase  $\gamma'$  in the matrix and  $\text{M}_{23}\text{C}_6$  carbide lamellae, and phase G particles on grain boundary

the matrix, whereas within the area of grain boundaries, the occurrence of  $\text{M}_{23}\text{C}_6$  carbide lamellae and lenticular particles of the G [ $\text{Ni}_{16}\text{Ti}_6\text{Si}_7$ ] intermetallic phase [10-12] were observed.

Research results of the Fe–Ni alloy strength and plasticity related properties in its initial state, i.e. after solution heat treatment and 1-stage ageing (variant A) and after solution heat treatment and 2-stage ageing at room temperature and at 600°C are quoted in Table 2. Based on the provided results it can be seen that the specimens subjected to 2-stage ageing (variant B) demonstrated better strength at room temperature. Also, at an increased temperature 600°C, variant B has shown higher Y.S and T.S values.

Table 2. Mechanical properties of the Fe–Ni alloy after ageing according to variants A and B

Variant of ageing	Test temperature [°C]	Y.S [MPa]	T.S [MPa]	EL. [%]	R.A [%]
A	20	701	1021	27	48
B		761	1097	26	46
A	600	611	802	12	39
B		698	879	11	37

Higher strength-related properties with the slightly lower plastic properties of the specimens after 2-stage ageing can be accounted for by stronger strengthening of grain boundaries and the zones near boundaries through precipitation of  $M_{23}C_6$  carbides and phase G [ $Ni_{16}Ti_6Si_7$ ] [10- 12].

The results of fatigue tests conducted at temperatures of 20°C on Fe–Ni alloy specimens heat treated according to variants A and B are provided in Table 3 and presented in Figs. 6 and 7. During the low-cycle fatigue tests for individual ranges of total strain  $\Delta\epsilon_t$  (0.6-1.4%), the values of amplitudal stress  $\sigma_a$  were determined depending on the number of cycles N.

Based on those data, graphs of cyclic softening were built and the values of saturation stress  $\sigma_{an}$  were determined for the studied alloy. As results from the low-cycle tests conducted at a temperature of 20°C, the specimens subjected to ageing according to variant A show higher fatigue durability, while the specimens aged according to variant B demonstrate higher stress saturation (Figs. 6, 7). In both variants of heat treatment, the Fe–Ni alloy is characterized by cyclic softening in the low-cycle fatigue conditions.

The results of low-cycle fatigue tests carried out at an elevated temperature of 600°C are provided in Table 4 and presented in Figs. 8 and 9.

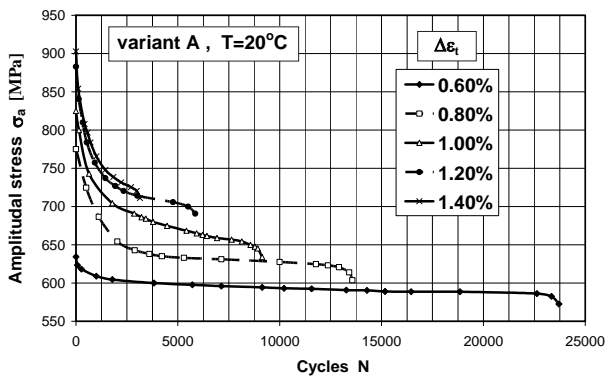


Fig. 6. Cyclic softening curves of the Fe–Ni alloy for variant A at a temperature 20°C

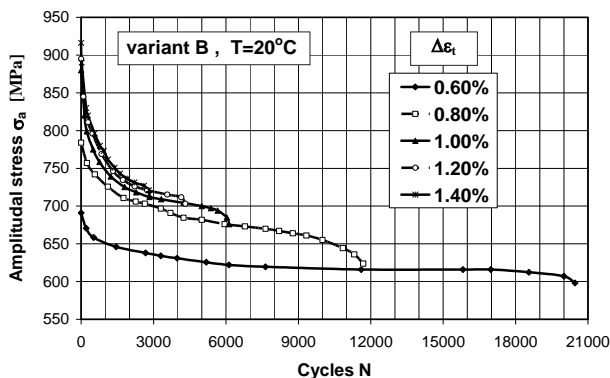


Fig. 7. Cyclic softening curves of the Fe–Ni alloy for variant B at a temperature 20°C

Table 3.

Results of low-cycle fatigue tests of the Fe–Ni alloy specimens, variants A and B at a temperature of 20°C

Variant of ageing	Ranges of strain			$\sigma_{an}$ [MPa]	$N_f$	
	$\Delta\epsilon_t$	$\Delta\epsilon_e$	$\Delta\epsilon_p$			
A	0.6%	0.006	0.0054	0.0006	593	23770
	0.8%	0.008	0.0060	0.0020	634	13520
	1.0%	0.010	0.0064	0.0036	677	9064
	1.2%	0.012	0.0068	0.0052	717	5820
	1.4%	0.014	0.0071	0.0069	744	3120
B	0.6%	0.006	0.0055	0.0005	611	20460
	0.8%	0.008	0.0064	0.0016	675	11740
	1.0%	0.010	0.0068	0.0032	712	6120
	1.2%	0.012	0.0072	0.0048	725	4320
	1.4%	0.014	0.0074	0.0066	737	2790

Table 4.

Results of Fe–Ni alloy low-cycle fatigue tests for variants A and B at a temperature of 600°C

Variant of ageing	Ranges of strain			$\sigma_{an}$ [MPa]	$N_f$	
	$\Delta\epsilon_t$	$\Delta\epsilon_e$	$\Delta\epsilon_p$			
A	0.8%	0.008	0.0069	0.0011	585	1440
	1.2%	0.012	0.0072	0.0048	610	432
B	0.8%	0.008	0.0064	0.0016	540	500
	1.2%	0.012	0.0071	0.0049	600	310

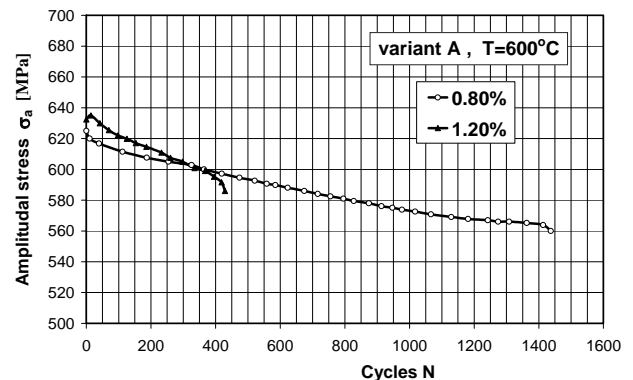


Fig. 8. Cyclic softening curves of the Fe–Ni alloy for variant A at a temperature 600°C

Based on the low-cycle tests conducted at a temperature of 600°C it was found that similarly to the tests at room temperature, the specimens aged according to variant A are characterized by higher fatigue durability (Fig. 8). The specimens subjected to 1-stage ageing demonstrate higher stress saturation  $\sigma_{an}$ . For both variants of heat treatment, the alloy becomes cyclically softened in low-cycle fatigue conditions. Particularly intense softening is observed in the alloy subjected to heat treatment following variant B, which decreases its operational usability in the conditions of cyclic fatigue at increased temperatures (Fig. 9).

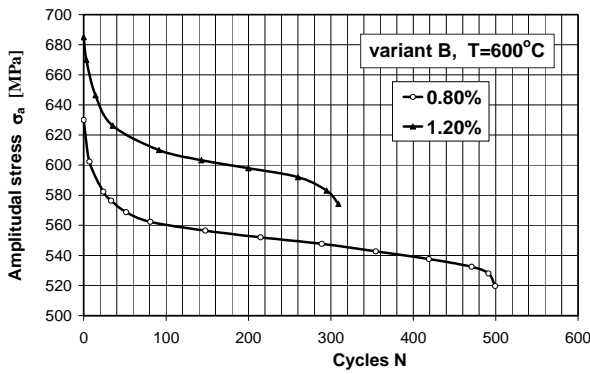


Fig. 9. Cyclic softening curves of the Fe–Ni alloy for variant B at a temperature 600°C

The ranges of plastic strain  $\Delta\varepsilon_p$  and elastic strain  $\Delta\varepsilon_e$ , and their corresponding stress range  $\Delta\sigma$ , were determined on the basis of a hysteresis loop recorded in the course of the testing. The results obtained were used to elaborate a fatigue durability graph of the studied alloy. The fatigue durability values for the Fe–Ni alloy at room temperature were described by the Smith, Hirschberg and Manson dependence [17]:

$$\Delta \varepsilon_t = \Delta \varepsilon_p + \Delta \varepsilon_e = M \cdot N_f^z + \frac{G}{E} \cdot N_f^v \quad (1)$$

where: M, G, E, z, v – material constants.

The results of the Fe–Ni alloy fatigue durability at room temperature are provided in Table 5 and illustrated in Figs. 10, 11.

An analysis of the Fe–Ni alloy fatigue durability graphs at room temperature has shown that for both ageing variants, A and B, the intersection point  $N_i$  of graphs  $\Delta\varepsilon_e=f(N_f)$  and  $\Delta\varepsilon_p=f(N_f)$  is located in the low-cycle range, i.e. 4000 and 3000 cycles, respectively (Figs. 10, 11). This testifies to the fact that the cyclic deformation process of the alloy was proceeding with a dominant participation of the elastic component  $\Delta\varepsilon_e$  within the complete strain ranges  $\Delta\varepsilon_t$  assumed for the tests (Table 3). In both of the studied ageing variants of the Fe–Ni alloy, the resistance to plastic deformation depends mainly on its strength-related properties.

A comparison of the influence of the Fe–Ni alloy’s both ageing variants on fatigue durability ( $N_f$ ) at room and increased temperatures is presented in Figs. 12 and 13. As can be seen from the data provided, both at a room temperature and at a temperature increased to 600°C, the alloy’s fatigue durability was higher for variant A compared to variant B.

Table 5. Mathematical models of the Fe–Ni alloy specimens’ fatigue durability for variant A and B at room temperature

Variant of ageing	$\Delta \varepsilon_p = M \cdot N_f^z$		$\Delta \varepsilon_e = (G/E) \cdot N_f^v$	
	M	z	G/E	v
A	126.0	-1.18	0.0217	-0.136
B	188.4	-1.27	0.0240	-0.144

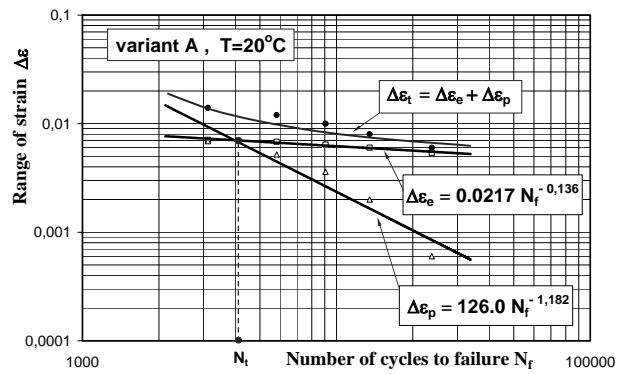


Fig. 10. Fatigue durability graphs of the Fe–Ni alloy for variant A at a temperature 20°C

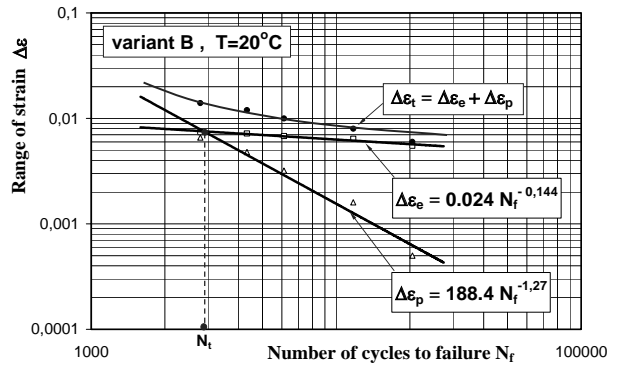


Fig. 11. Fatigue durability graphs of the Fe–Ni alloy for variant B at a temperature 20°C

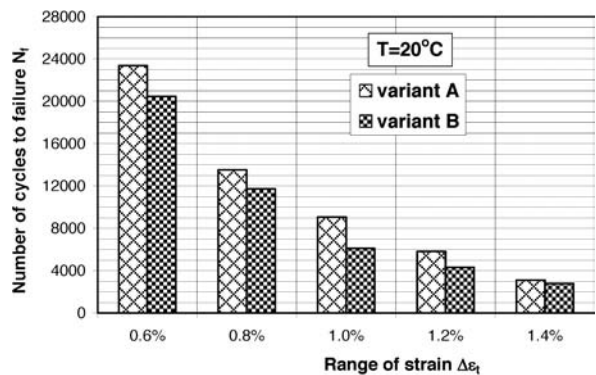


Fig. 12. Comparison of fatigue durability of ageing variants A and B for the Fe–Ni alloy at room temperature

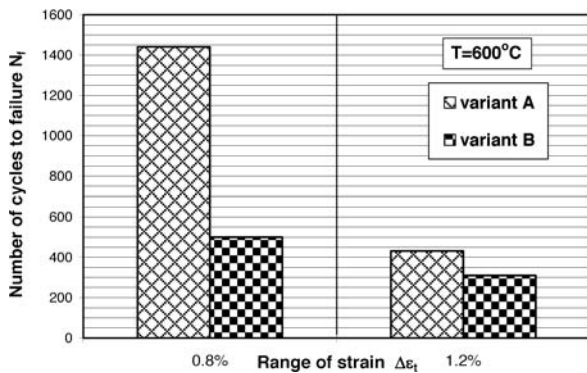


Fig. 13. Comparison of fatigue durability of ageing variants A and B for the Fe–Ni alloy at an increased temperature of 600°C

Having obtained the saturation stress values  $\sigma_{an}$  for amplitudal plastic strain  $\epsilon_p$ , mathematical models (2) of cyclic alloy deformation were devised, as given in Table 6 and presented graphically in Fig. 14. Also, a cyclic strength coefficient ( $K'$ ) and a cyclic weakening exponent ( $n'$ ) were determined for the studied alloy [17]:

$$\sigma_n = K' \cdot \left[ \frac{\epsilon_p}{2} \right]^{n'} \quad (2)$$

where:  $K'$  – cyclic strength coefficient,  $n'$  – cyclic softening exponent.

Fractographic observations were conducted on the Fe–Ni specimen fractures after tensioning and after low-cycle fatigue at room temperature and an increased temperature of 600°C. The results of studies for both variants of heat treatment are presented in Figs. 15–20. In variant A specimens after 1-stage ageing and tensioning at room temperature, a transcrystalline ductile fracture with traces of significant plastic strain was found (Fig. 15). In variant B specimens after 2-stage ageing and analogical tensioning, a similar type of ductile fracture was observed, however with a minor fraction of intergranular cracks (Fig. 16).

Table 6. Values of coefficient ( $K'$ ) and exponents ( $n'$ ) for the Fe–Ni alloy deformation curves at 20°C of variants A and B

Variant of ageing	$\epsilon_p$	$\sigma_{an}$ [MPa]	$K'$ [MPa]	$n'$
A	0.0003	593	1233.2	0.092
	0.0010	634		
	0.0018	677		
	0.0026	717		
	0.0034	744		
B	0.0025	611	1131.7	0.074
	0.0008	675		
	0.0016	712		
	0.0024	725		
	0.0033	737		

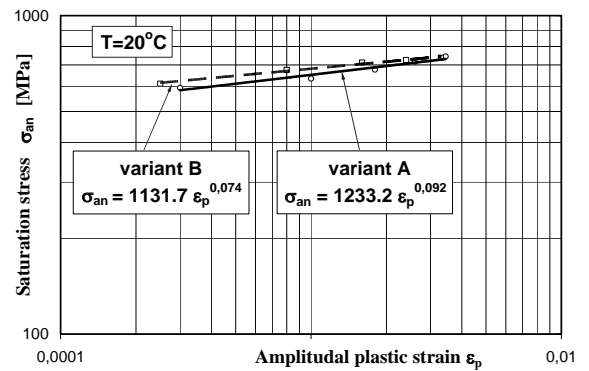


Fig. 14. Cyclic deformation graph of the specimens for ageing variants A and B of the Fe–Ni alloy at room temperature

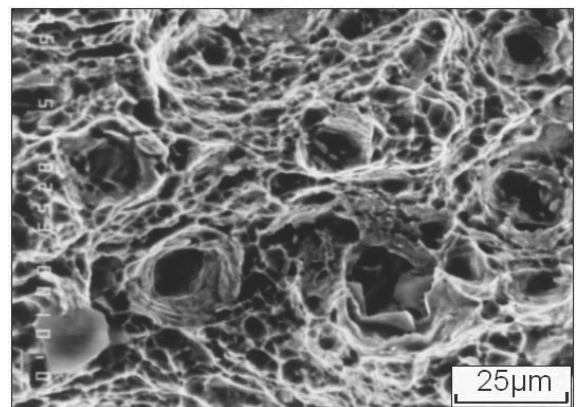


Fig. 15. Variant A specimen fracture after tensioning at a temperature of 20°C. Transcrystalline ductile fracture

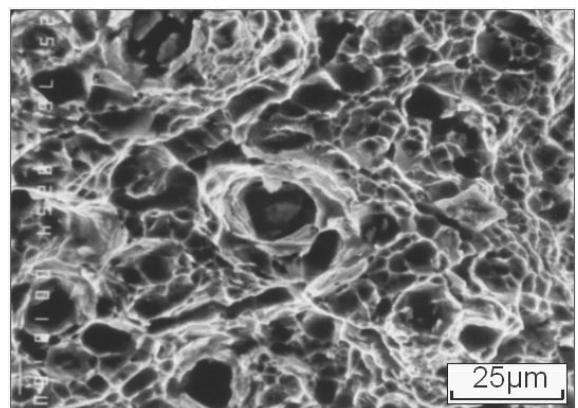


Fig. 16. Variant B specimen fracture after tensioning at a temperature of 20°C. Transcrystalline ductile fracture with cleavage cracks

After low-cycle fatigue tests conducted until total strain  $\Delta\epsilon_t=0.8\%$  at room temperature, the specimens demonstrated a certain diversification in terms of the obtained fractures' morphology (Fig. 17, 18). In variant A specimens, a typical fatigue fracture with characteristic fatigue stripes and traces of significant plastic deformation were observed (Fig. 17). In the case of variant B specimens, the fatigue fracture was of a cleavage type, with a fraction of intergranular cracks and traces of slight plastic strain (Fig. 18).

Also, after low-cycle fatigue tests conducted until total strain  $\Delta\epsilon_t=1.2\%$  at an increased temperature of  $600^\circ\text{C}$ , the specimens demonstrated significant diversification in terms of the obtained fractures' morphology (Figs. 19 and 20). In variant A specimens, a mixed fatigue fracture with trace fatigue stripes and minor plastic deformation was observed (Fig. 19). In the case of variant B specimens, the intercrystalline fracture did not reveal any features of fatigue fracture (Fig. 20). The occurrence of this type of fracture in low-cycle fatigue tests at a temperature of  $600^\circ\text{C}$  proves the material's substantial brittleness in variant B specimens at increased temperatures.

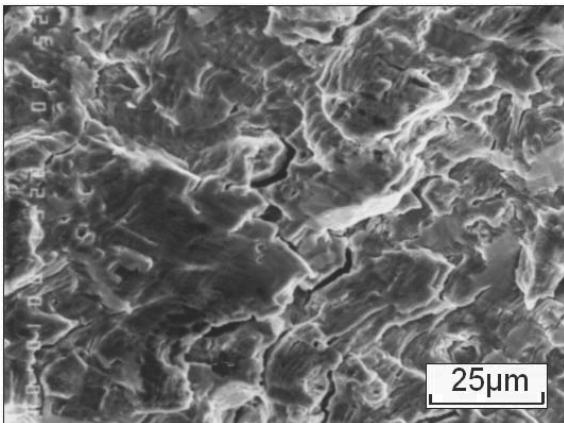


Fig. 17. Variant A specimen fatigue fracture after fatigue tests ( $\Delta\epsilon_t=0.8\%$ ) at a temperature of  $20^\circ\text{C}$ . Transcrystalline ductile fracture

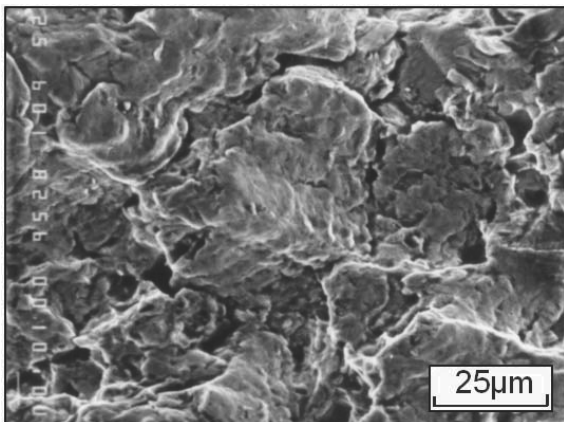


Fig. 18. Variant B specimen fatigue fracture after fatigue tests ( $\Delta\epsilon_t=0.8\%$ ) at a temperature of  $20^\circ\text{C}$ . Mixed transcrystalline fracture

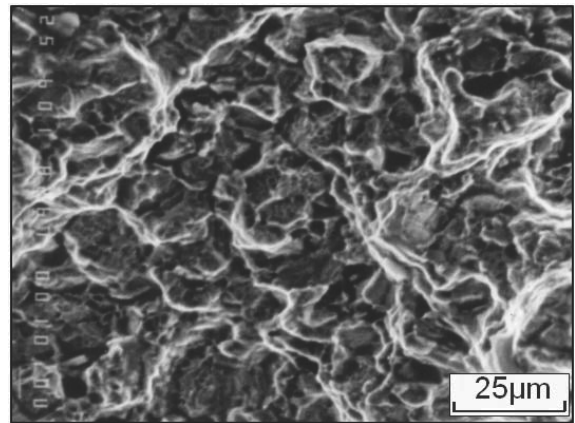


Fig. 19. Variant A specimen fatigue fracture after fatigue tests ( $\Delta\epsilon_t=1.2\%$ ) at a temperature of  $600^\circ\text{C}$ . Mixed intercrystalline fracture

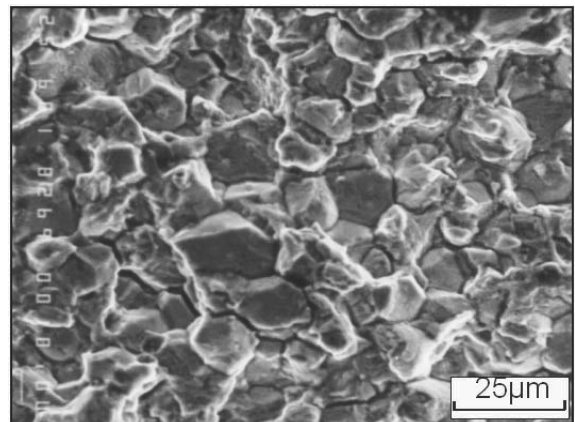


Fig. 20. Variant B specimen fatigue fracture after fatigue tests ( $\Delta\epsilon_t=1.2\%$ ) at a temperature of  $600^\circ\text{C}$ . Intercrystalline fracture

## 4. Conclusions

The paper analyses the influence of initial heat treatment on the mechanical properties and structure of the austenitic Fe–Ni alloy precipitation-strengthened with intermetallic phases of the  $\gamma'$   $[\text{Ni}_3(\text{Al},\text{Ti})]$  type. Specimens of the studied alloy after solution heat treatment ( $980^\circ\text{C}/2\text{h}/\text{water}$ ) were subjected to two ageing variants, i.e. 1-stage ageing ( $715^\circ\text{C}/16\text{h}/\text{air}$ ) – variant A and 2-stage ageing ( $715^\circ\text{C}/8\text{h}/\text{furnace} + 650^\circ\text{C}/8\text{h}/\text{air}$ ) – variant B. On heat-treated specimens according to variants A and B, static tensile test and low-cycle fatigue test were performed in the range  $\Delta\epsilon_t=0.6\text{--}1.4\%$  at temperatures of 20 and  $600^\circ\text{C}$ .

Static tensile tests conducted at a temperature of  $20^\circ\text{C}$  demonstrated higher strength properties of the specimens for variant B ( $Y.S = 761\text{ MPa}$ ,  $T.S = 1097\text{ MPa}$ ) compared to variant A ( $Y.S = 701\text{ MPa}$ ,  $T.S = 1021\text{ MPa}$ ), with their plastic properties being comparable. Also, at a temperature of  $600^\circ\text{C}$ , variant B specimens were characterized by higher strength properties

(Y.S = 698 MPa, T.S = 879 MPa) in comparison with variant A (Y.S = 611 MPa, T.S = 802 MPa).

The low-cycle fatigue tests proved a significant influence of the applied ageing variants A and B on the Fe–Ni alloy's fatigue durability at room temperature and at 600°C. At both temperatures tested, the alloy's fatigue durability after thermal treatment according to variant A was higher than the durability of the alloy treated according to variant B, whereas greater differences between the durability values (by ca. 70%) were observed at a temperature of 600°C. In the studies conducted at room temperature, the greatest differences in fatigue durability (in the range of 13-32%) occurred in the range of total strain of 0.8-1.2%.

The reason for lower fatigue durability at temperatures of 20 and 600°C of the heat treated specimens in variant B should be sought in a larger number of secondary phase particles precipitated on grain boundaries, which determines earlier initiation of the fatigue cracking process. This has been corroborated by the observation of the fatigue fractures' morphology, where a development of intergranular cracks was found, indicating low cohesion of the grain boundaries, especially at a temperature of 600°C.

The analysis of the Fe–Ni alloy's fatigue durability graphs at room temperature has shown that for the ageing variants A and B, the intersection point  $N_f$  of the graphs  $\Delta\epsilon_e=f(N_f)$  and  $\Delta\epsilon_p=f(N_f)$  is located in the low-cycle range (3000-4000 cycles). This testifies to the fact that the cyclic deformation process of the alloy was proceeding with a dominant participation of the elastic component  $\Delta\epsilon_e$  within the total strain ranges assumed in the studies. In such conditions, the investigated alloy's fatigue durability for both ageing variants was determined by its strength properties.

On the basis of the results obtained, a conclusion can be drawn that the studied Fe–Ni alloy is characterized by better material characteristics after solution heat treatment and 1-stage ageing at 715°C/16h/air. With its slightly decreased strength properties, the alloy heat treated according to variant A shows definitely higher durability in the conditions of low-cycle fatigue, especially at elevated temperatures.

## References

- [1] M. Konter, M. Thumann, Materials and manufacturing of advanced industrial gas turbine components, *Journal of Materials Processing Technology* 117 (2001) 386-390.
- [2] R. Shargi-Moshtaghin, S. Asgari, The influence of thermal exposure on the  $\gamma'$  precipitates characteristics and tensile of superalloy IN-738LC, *Journal of Materials Processing Technology* 147 (2004) 343-350.
- [3] S.A. Sajjadi, S.M. Zebarjad, Effect of temperature on tensile fracture mechanisms of a Ni-base superalloy, *Archives of Materials Science and Engineering* 28/1 (2007) 34-40.
- [4] S.A. Sajjadi, S.M. Zebarjad, Study of fracture mechanisms of a Ni-Base superalloy at different temperatures, *Journal of Achievements in Materials and Manufacturing Engineering* 18 (2006) 227-230.
- [5] P. Jonsta, Z. Jonsta, J. Sojka, L. Cizek, A. Hernas, Structural characteristics of nickel superalloy Inconel 713LC after heat treatment, *Journal of Achievements in Materials and Manufacturing Engineering* 21/2 (2007) 29-32.
- [6] N.S. Stoloff, Wrought and P/M superalloys, *ASM Handbook, Vol. 1: Properties and Selection Irons, Steels and High-Performance Alloys*, ASM Materials Information Society, Ohio, 1990, 950-977.
- [7] F. Schubert, Temperature and Time Dependent Transformation: Application to Heat Treatment of High Temperature Alloys, In: *Phase Stability in High Temperature Alloys*, Applied Science Publishers LTD, London, 1981, 119-149.
- [8] Ch.T. Sims, N.S. Stoloff, W.C. Hagel, *Superalloys II*, Ed.A. Wiley Interscience Publications, New York, 1987.
- [9] K.J. Ducki, M. Hetmańczyk, The influence of prolonged aging on the structure and properties of precipitation hardened austenitic alloy, *Materials Engineering* 4 (2001) 290-293.
- [10] K.J. Ducki, Analysis of the precipitation and growth processes of intermetallic phase in a high-temperature Fe–Ni alloy, *Materials Engineering* 2 (2007) 53-58 (in Polish).
- [11] K.J. Ducki, Structure and precipitation strengthening in a high-temperature Fe–Ni alloy, *Archives of Materials Science and Engineering* 28/4 (2007) 203-210.
- [12] K.J. Ducki, Analysis of the structure and precipitation strengthening in a creep resisting Fe–Ni alloy, *Journal of Achievements in Materials and Manufacturing Engineering* 21/2 (2007) 25-28.
- [13] J. Okrajni, M. Cieśla, L. Swadźba, High-temperature low-cycle fatigue and creep behaviour of nickel-based superalloys with heat-resistant coating, *Fatigue and Fracture of Materials and Engineering Structures* 21 (1998) 947-954.
- [14] Z. Gronostajski, K. Jaśkiewicz, Influence of monotonic and cyclic deformation sequence on behaviour of CuSi3.5 silicon bronze, *Journal of Achievements in Materials and Manufacturing Engineering* 15 (2006) 39-46.
- [15] J. Okrajni, A. Marek, G. Junak, Description of the deformation process under thermo-mechanical fatigue, *Journal of Achievements in Materials and Manufacturing Engineering* 21/2 (2007) 15-23.
- [16] J. Okrajni, A. Marek, G. Junak, Stress-strain characteristics under mechanical and thermal loading, *Journal of Achievements in Materials and Manufacturing Engineering* 20 (2007) 271-274.
- [17] S. Kocańda, A fatigue cracking of metals, WNT, Warsaw, 1985 (in Polish).